Neuron
Article

Zinc Dynamics and Action at Excitatory Synapses

Angela Maria Vergnano,[1,2,3,8] Nelson Rebola,[4,5,8] Leonid P. Savtchenko,[6,8] Paulo S. Pinheiro,[4,5] Mariano Casado,[1,2,3] Brigitte L. Kieffer,[7] Dmitri A. Rusakov,[6] Christophe Mulle,[4,5,9,*] and Pierre Paoletti[1,2,3,9,*]
[1]Ecole Normale Supérieure, Institut de Biologie de l'ENS (IBENS), F-75005 Paris, France
[2]Inserm, U1024, F-75005 Paris, France
[3]CNRS, UMR 8197, F-75005 Paris, France
[4]Université de Bordeaux, Institut Interdisciplinaire de Neurosciences, F-33000 Bordeaux, France
[5]CNRS UMR 5297, F-33000 Bordeaux, France
[6]UCL Institute of Neurology, University College London, London, WC1N 3BG, UK
[7]Institut de Génétique et de Biologie Moléculaire et Cellulaire, Université de Strasbourg, CNRS, INSERM, 67404 Illkirch, France
[8]Co-first author
[9]Co-senior author
*Correspondence: mulle@u-bordeaux2.fr (C.M.), pierre.paoletti@ens.fr (P.P.)
http://dx.doi.org/10.1016/j.neuron.2014.04.034

SUMMARY

Decades after the discovery that ionic zinc is present at high levels in glutamatergic synaptic vesicles, where, when, and how much zinc is released during synaptic activity remains highly controversial. Here we provide a quantitative assessment of zinc dynamics in the synaptic cleft and clarify its role in the regulation of excitatory neurotransmission by combining synaptic recordings from mice deficient for zinc signaling with Monte Carlo simulations. Ambient extracellular zinc levels are too low for tonic occupation of the GluN2A-specific nanomolar zinc sites on NMDA receptors (NMDARs). However, following short trains of physiologically relevant synaptic stimuli, zinc transiently rises in the cleft and selectively inhibits postsynaptic GluN2A-NMDARs, causing changes in synaptic integration and plasticity. Our work establishes the rules of zinc action and reveals that zinc modulation extends beyond hippocampal mossy fibers to excitatory SC-CA1 synapses. By specifically moderating GluN2A-NMDAR signaling, zinc acts as a widespread activity-dependent regulator of neuronal circuits.

INTRODUCTION

Zinc is abundant in the body. Although the vast majority of zinc ions are trapped within proteins as structural or catalytic cofactors, in the mammalian brain, a pool of loosely bound (or chelatable) zinc shows a restricted distribution in telencephalic regions (hippocampus, cortex, striatum, and amygdala). Chelatable zinc is localized almost exclusively within synaptic vesicles in a subset of glutamatergic terminals, where it is accumulated by the vesicular zinc transporter ZnT3 (Frederickson et al., 2000; Paoletti et al., 2009; Sensi et al., 2009; Sindreu and Storm, 2011). The increased availability of selective zinc-sensitive fluorescent probes, novel zinc chelators, and genetically modified animal models has clearly established zinc as a pleiotropic modulator of intracellular and intercellular neuronal signaling in physiological and pathological aspects of brain function (Adlard et al., 2010; Carter et al., 2011; Hirzel et al., 2006; Koh et al., 1996; Martel et al., 2010, 2011; Nozaki et al., 2011; Sindreu et al., 2011). Yet, the conditions under which vesicular zinc is released during synaptic activity and its functional significance remain largely enigmatic.

Extracellular zinc interacts with various neuronal ion channels, receptors, and transporters and therefore can modulate synaptic transmission (Grauert et al., 2014; Mott et al., 2008; Paoletti et al., 2009; Smart et al., 2004; Veran et al., 2012). Depending on the target, zinc can exert either positive or negative modulatory effects, with varying potency. NMDA-type glutamate receptors (NMDARs) stand out for their exquisite and complex zinc sensitivity. Zinc concentrations as low as 10–20 nM produce marked inhibition of NMDARs through an allosteric mechanism involving a high-affinity zinc site in the N-terminal domain (NTD) of the GluN2A subunit (Chen et al., 1997; Choi and Lipton, 1999; Fayyazuddin et al., 2000; Gielen et al., 2008; Low et al., 2000; Paoletti et al., 1997; Paoletti et al., 2000; Traynelis et al., 1998; Williams, 1996). Zinc also binds the homologous NTD of GluN2B and inhibits GluN2B-containing receptors, although with lower affinity (IC_{50} ~2 μM) (Karakas et al., 2009; Rachline et al., 2005; Traynelis et al., 1998). An additional effect of zinc at NMDARs is a voltage-dependent channel block that occurs in the 10–50 μM range (IC_{50} ~30 μM at −60 mV) and affects, without distinction, both GluN2A- and GluN2B-containing receptors (Paoletti et al., 1997).

The abundance of potential synaptic targets and the presence of chelatable zinc in synaptic vesicles all point to a role for zinc as a modulator of synaptic transmission. Yet, the extracellular dynamics of zinc released in the synaptic cleft is highly controversial even at hippocampal mossy fiber (MF) synapses, which are the most zinc-enriched fibers in the brain. Estimations of peak zinc concentrations in the synaptic cleft following exocytosis spans more than three orders of magnitude, from low nanomolars to high micromolars (>100 μM) (Aniksztejn et al., 1987; Assaf and Chung, 1984; Besser et al., 2009; Frederickson et al., 2006a; Howell et al., 1984; Kay, 2003; Kodirov et al., 2006; Komatsu

et al., 2005; Li et al., 2001; Molnár and Nadler, 2001; Qian and Noebels, 2005, 2006; Ueno et al., 2002; Vogt et al., 2000). The very fact that zinc freely diffuses after exocytosis has even been challenged by the suggestion that vesicular zinc is externalized but sticks to the presynaptic membrane, forming a so-called "zinc-veneer" (Kay, 2003; Kay and Tóth, 2008; Nydegger et al., 2010).

Several reasons make the study of brain zinc a difficult task. Perturbing endogenous zinc concentrations, as done in many past studies, produces pleiotropic effects, in accordance with the multiplicity of zinc targets (for review, see Paoletti et al., 2009; Smart et al., 2004). Tools to manipulate zinc levels also have important drawbacks. In particular, most zinc-chelating agents also bind calcium, thus interfering with synaptic transmission. Those that do not affect calcium levels (such as CaEDTA) are usually too slow to buffer zinc with kinetics compatible with fast synaptic transmission (Pan et al., 2011; Paoletti et al., 2009). Determining the levels of ambient zinc as well as the magnitude and duration of the potential zinc concentration transients in the synaptic cleft after exocytosis is of primary importance in evaluating the neuromodulatory role of this divalent cation. To address these issues, we have exploited our recently created GluN2A-H128S knockin (KI) mice, in which the high-affinity zinc inhibition of NMDARs is specifically eliminated (Nozaki et al., 2011). Comparing NMDAR-mediated currents in different conditions of synaptic activity in wild-type, KI, as well as ZnT3 knockout (ZnT3 KO) (Cole et al., 1999) and GluN2A knockout (GluN2A KO) (Sakimura et al., 1995) mice, we probed the zinc-containing synaptic microenvironment around NMDARs. In addition, we tested zinc release, diffusion, and receptor action in the synaptic cleft by employing a detailed Monte Carlo model of the excitatory synapses under study. We present evidence that, at both MF-CA3 and Schaffer collateral (SC)-CA1 synapses, zinc acts as a bona fide neuromodulator that is released via exocytosis and diffuses in the synaptic cleft specifically interacting with postsynaptic GluN2A-NMDARs, thus contributing to activity-dependent synaptic integration and plasticity.

RESULTS

Selective Abrogation of Nanomolar Zinc Inhibition of NMDARs in GluN2A-H128S KI Mice

Because NMDARs contain dedicated zinc-binding sites capable of sensing extracellular zinc over a wide concentration range (Paoletti et al., 2009), measuring NMDAR activity provides a sensitive mean to assess for the presence and physiological actions of zinc in the synaptic cleft. We first evaluated the sensitivity of synaptic NMDARs to exogenous zinc by recording NMDAR-mediated excitatory postsynaptic currents (NMDA-EPSCs) at two distinct glutamatergic synapses in acute hippocampal slices. NMDARs in the hippocampus are mostly composed of GluN2A and GluN2B subunits (Paoletti et al., 2013), which confer low nanomolar and low micromolar zinc sensitivity, respectively (Paoletti et al., 2009). In order to precisely control zinc concentrations in the extracellular milieu, we used the chelator tricine (10 mM) to buffer zinc (Paoletti et al., 1997; see Experimental Procedures). In agreement with the presence of GluN2A-containing NMDARs, application of 100 nM free zinc in slices from wild-type (WT) mice produced significant inhibition of NMDA-EPSCs both at SC-CA1 and MF-CA3 synapses (Figures 1A and 1D; mean inhibition of 22% ± 6% [n = 5] and 35% ± 5% [n = 5], respectively, p = 0.025 and 0.007, respectively, Student's paired t test). This inhibition was absent in slices from GluN2A-H128S KI mice (Figures 1A and 1D; SC-CA1: 2% ± 2% [n = 6]; MF-CA3: 7% ± 5% [n = 8], p > 0.05), as expected from the lack of high-affinity zinc inhibition of NMDARs in these animals (Nozaki et al., 2011). Zinc (300 nM) had no effect on AMPA-EPSCs in either WT or KI slices (Figure S1 available online), as expected from the very low zinc sensitivity of AMPARs (Mott et al., 2008; Paoletti et al., 2009).

The full zinc dose-response curves revealed that, at both MF-CA3 and SC-CA1 synapses, the sensitivity of KI NMDA-EPSCs to extracellular zinc was greatly reduced in the nanomolar, but not the micromolar, concentration range (Figures 1B and 1E). This agrees with the strong (~1,000-fold), but not total, decrease in zinc sensitivity produced by the GluN2A-H128S mutation in recombinant GluN2A-NMDARs (Fayyazuddin et al., 2000). The presence of GluN2B-NMDARs with low micromolar zinc sensitivity (Karakas et al., 2009; Rachline et al., 2005) is also likely to account for the residual micromolar zinc sensitivity observed in the KI animals. In parallel to its potent inhibitory action on peak NMDA-EPSCs from WT slices, zinc applied in the nanomolar range prolonged WT NMDA-EPSC decay kinetics (Figures 1C and 1F). This prolongation is expected from the reduced contribution of fast-decaying GluN2A-NMDARs and the slowing down of glutamate deactivation kinetics upon zinc binding to GluN2A-NMDARs (Erreger and Traynelis, 2005; Paoletti et al., 1997; Tovar and Westbrook, 2012; Zheng et al., 2001). In KI slices, NMDA-EPSC kinetics were not affected by nanomolar zinc concentrations (Figures 1C and 1F), in agreement with the lack of zinc binding to the mutated GluN2A NTD. Overall, these results show that the introduction of the GluN2A-H128S mutation leads to a selective loss of the high-affinity zinc inhibition of NMDARs. While NMDARs from KI animals are impaired in sensing nanomolar zinc concentrations, they remain sensitive to zinc levels in the low micromolar range. Thus, NMDARs embedded in their native synaptic environment are highly sensitive to extracellular zinc as their recombinant counterparts and zinc binding to the GluN2A NTD accounts for this high zinc sensitivity.

No Tonic Zinc Inhibition of Synaptic NMDARs in Normal Mg^{2+} Conditions

We next aimed at evaluating the levels of endogenous zinc in the synaptic cleft under resting conditions. At MF-CA3 synapses, it has been proposed that ambient zinc levels are sufficient to permanently occupy the GluN2A-specific high-affinity zinc-binding site of NMDARs, resulting in tonic inhibition of NMDA-EPSCs (Vogt et al., 2000). We reinvestigated the issue of ambient synaptic zinc levels by exploiting GluN2A-H128S KI mice in which NMDARs fail to detect nanomolar, but not micromolar, zinc concentrations. We evaluated the influence of bath application of zinc chelators on MF-CA3 NMDA-EPSCs evoked by low-frequency (0.1 Hz) stimulation and recorded in either one of two conventional experimental conditions: at a negative membrane potential in low Mg^{2+} concentrations and at a positive membrane potential in normal Mg^{2+} concentrations. In low Mg^{2+},

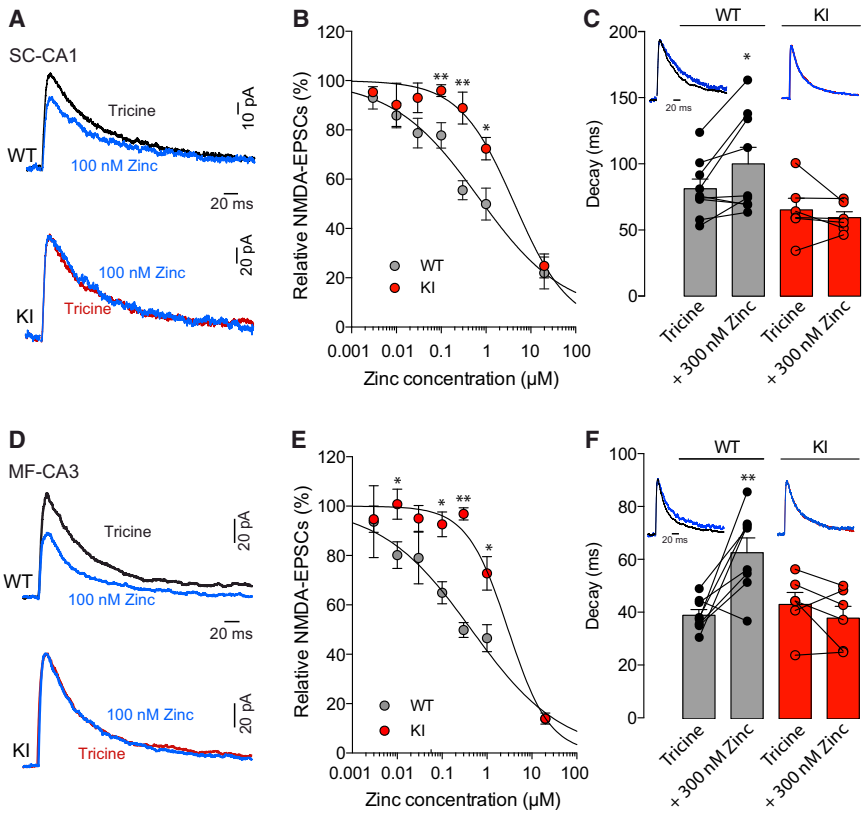

Figure 1. Loss of High-Affinity Zinc Inhibition of NMDA-EPSCs in GluN2A-H128S KI Mice

(A) Representative traces of SC-CA1 NMDA-EPSCs illustrating the effects of 100 nM free zinc application on NMDA-EPSCs in WT and KI mice. The inhibition observed in WT mice is absent in KI mice.

(B) Concentration-response curves of zinc inhibition of SC-CA1 NMDA-EPSCs in WT and KI mice. Each point is the mean value from 3–9 cells.

(C) Decay kinetics of SC-CA1 NMDA-EPSCs in control conditions (+ tricine) and after 300 nM free zinc application. Zinc increased the decay kinetics of NMDA-EPSCs in WT but not KI mice. Insets: superimposed NMDA-EPSCs with and without zinc (normalized traces).

(D) Representative traces of MF-CA3 NMDA-EPSCs illustrating the effect of 100 nM free zinc application in WT and KI mice. The inhibition observed in WT mice is absent in KI mice.

(E) Concentration-response curves of zinc inhibition of MF-CA3 NMDA-EPSCs in WT and KI mice. Each point is the mean value from 4–8 cells.

(F) Decay kinetics of WT and KI MF-CA3 NMDA-EPSCs in control conditions (+ tricine) and after 300 nM free zinc application. Insets: superimposed NMDA-EPSCs with and without zinc (normalized traces). Data are presented as mean ± SEM. *$p < 0.05$, **$p < 0.01$, Student's paired t test. See also Figure S1 for zinc effects on AMPA-EPSCs.

application of 2 mM CaEDTA, a widely used zinc chelator (Kay and Tóth, 2008; Koh et al., 1996; Paoletti et al., 2009), markedly increased WT NMDA-EPSCs (171% ± 20% [n = 9]; Figure 2A), confirming previous results (Vogt et al., 2000) and indicating the presence of endogenous zinc at MF-CA3 synapses, which inhibits NMDARs. In contrast, CaEDTA had no effect on KI NMDA-EPSCs (115% ± 11% [n = 13]; Figure 2A), revealing that endogenous zinc levels in the MF-CA3 synaptic cleft are in the sub-μM range. Application of 10 mM tricine produced similar effects (WT 170% ± 50% [n = 8]; KI 87% ± 11% [n = 8]; Figure 2A). Because a slow (CaEDTA) and a fast (tricine) zinc chelator show strikingly similar effects, it is likely that MF-CA3 NMDARs are subjected to tonic (ambient) zinc inhibition. Interestingly, the effects of both CaEDTA and tricine were highly variable from cell to cell, with only ~50% of the cells showing a clear potentiation (Figure S2A). At SC-CA1 synapses, no significant effect on WT or KI NMDA-EPSCs by CaEDTA or tricine was observed, although in WT slices a few outlier cells did show marked potentiation (Figures S2B, S2C, and S2E). We interpret this variability, both at SC-CA1 and MF-CA3 synapses, as reflecting variable levels of extracellular ambient zinc in low Mg^{2+} conditions.

We next recorded synaptic NMDAR-mediated currents at positive potentials (+40 mV) in physiological Mg^{2+} (1.0–1.3 mM). In such conditions, CaEDTA produced no potentiation of NMDA-EPSCs at MF-CA3 synapses, as previously reported (Vogt et al., 2000), or at SC-CA1 synapses. Strikingly, tricine was also ineffective, and the effects of both chelators were indistinguishable between WT and KI (Figure 2B and Figures S2D and S2E). Because the high-affinity zinc inhibition of NMDARs is voltage independent (Paoletti et al., 1997), a tonic inhibitory action of zinc on NMDAR-GluN2A sites should be observed irrespective of the membrane potential. The differential effects of the chelators between negative and positive potentials could then originate from differing Mg^{2+} concentrations. We tested this hypothesis by recording MF-CA3 NMDA-EPSCs at −50 mV in normal Mg^{2+} or at +40 mV in low Mg^{2+}. In the first condition, no chelator effect was detected on either WT or KI mice (Figure S2A). In the second condition, CaEDTA and tricine both potentiated NMDA-EPSCs in WT but not KI mice (WT, CaEDTA: 141% ± 27% [n = 7]; tricine: 113% ± 10% [n = 8]; KI, CaEDTA: 73% ± 9% [n = 7]; tricine: 64% ± 7% [n = 9]; Figure 2C and Figure S2A). This indicates that ambient levels of zinc sensed by GluN2A sites results from the use of low Mg^{2+} concentrations, which may artificially increase ambient zinc levels by enhancing neuronal excitability (Mody et al., 1987) and thus vesicular zinc release. In slices from ZnT3 KO and GluN2A KO mice, CaEDTA or tricine no longer potentiated NMDA-EPSCs recorded in low Mg^{2+} (ZnT3 KO, 92% ± 10% [n = 6]; GluN2A KO, 77% ± 9% [n = 6]; Figure S2A), providing evidence that tonic zinc levels present in low Mg^{2+} conditions are in the sub-μM range and related to exacerbated synaptic activity.

These results unveil that in normal Mg^{2+} conditions, extracellular zinc levels present at rest in the synaptic cleft are in minute amounts (<10 nM), insufficient to populate the high-affinity (nM) zinc-binding sites on GluN2A-containing NMDARs. The absence of tonic zinc inhibition of synaptic NMDARs in normal

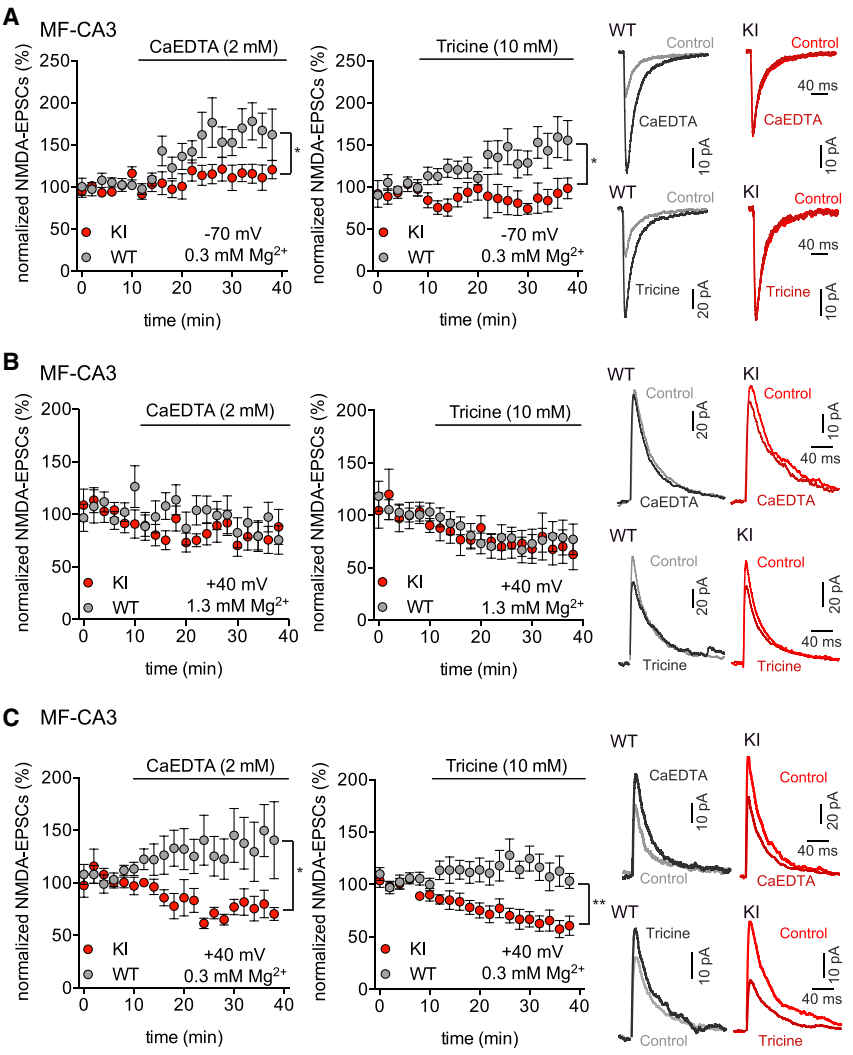

Figure 2. No Tonic Zinc Inhibition of Synaptic NMDARs in Normal Mg^{2+} Conditions

(A) Application of the zinc chelators CaEDTA and tricine increased MF-CA3 NMDA-EPSCs in WT but not KI mice in low extracellular Mg^{2+} (0.3 mM) conditions. Time courses and representative traces are shown. Recordings were performed at −70 mV.

(B) Lack of potentiating effect of the zinc chelators on MF-CA3 NMDA-EPSCs in normal extracellular Mg^{2+} (1.3 mM) and at +40 mV.

(C) In WT slices, the potentiation of MF-CA3 NMDA-EPSCs by the zinc chelators was recovered at positive potentials while recording in low extracellular Mg^{2+}. No potentiation was detected in slices from KI mice. Data are presented as mean ± SEM. *$p < 0.05$, **$p < 0.01$, Mann-Whitney test. See also Figure S2 for chelator effects at SC-CA1 NMDA-EPSCs and summary plot of single-cell values at both synapses.

Mg^{2+} conditions was further supported by the lack of difference in the NMDA/AMPA ratio and NMDA-EPSC decay kinetics between WT and KI mice (Figure S3).

Zinc Release and Modulation of MF-CA3 NMDA-EPSCs by Bursts of Synaptic Stimulations

Whether zinc freely diffuses in the extracellular space like a classical neurotransmitter is still intensely debated (Frederickson et al., 2000; Kay and Tóth, 2008; Paoletti et al., 2009; Sensi et al., 2009). Our previous results with the fast zinc chelator tricine (Figure 2B) clearly indicate that a single synaptic event is unable to produce zinc modulation of the related NMDA-EPSC at MF-CA3 synapses, despite the presence of highly zinc-sensitive NMDARs. This is in line with previous simulations predicting little impact of zinc coreleased with glutamate on NMDAR-mediated currents during individual synaptic responses (Erreger and Traynelis, 2005). In physiological situations, hippocampal granule cells fire in small bursts of action potentials (Jung and McNaughton, 1993). We thus applied bursts of presynaptic MF stimulation consisting of a short train of seven stimuli each separated by 40 ms (25 Hz) in normal Mg^{2+} conditions. As expected from the robust short-term plasticity of MF-CA3 synapses (Schmitz et al., 2001), such bursts resulted in a massive increase of NMDA-EPSC amplitude during the course of the train (ratio between the seventh and first pulse of 334% ± 37% [n = 15], for WT animals; Figure 3A). In slices from KI mice, the same protocol produced an even greater enhancement of synaptic NMDA-currents (ratio seventh/first, 472% ± 49% [n = 15], Figure 3A), pointing to an inhibitory action of synaptically released zinc on WT MF-CA3 NMDARs. Importantly, the gradual increase in AMPA-EPSCs during the train did not differ between WT and KI (Figure S4A), excluding changes in MF-CA3 short-term plasticity as the underlying cause of the difference between WT and KI NMDA-EPSCs.

Detailed comparison of the behavior of WT and KI NMDA-EPSCs during the trains also revealed that the difference between the two genotypes was most evident after the fourth pulse (Figure 3A), suggesting that at least four sequential synaptic events close in time are required for MF zinc to manifest its effect on postsynaptic NMDARs. We obtained further evidence that coreleased zinc is responsible for modulating NMDAR responses during the train by repeating the experiments in extracellular tricine. In presence of the fast zinc chelator, differences between WT and KI NMDA-EPSCs were abolished (Figure 3B), consistent with tricine intercepting zinc in transit within the synaptic cleft. In ZnT3 KO mice, NMDA-EPSCs continuously increased in amplitude during trains of seven stimuli at 25 Hz (Figure 3C), differing from the pattern observed in WT littermates but resembling the pattern observed in KI mice (ratio seventh/first of 557% ± 81% [n = 14] for ZnT3 KO animals; 325% ± 45% [n = 13] for WT littermate controls). Furthermore, the

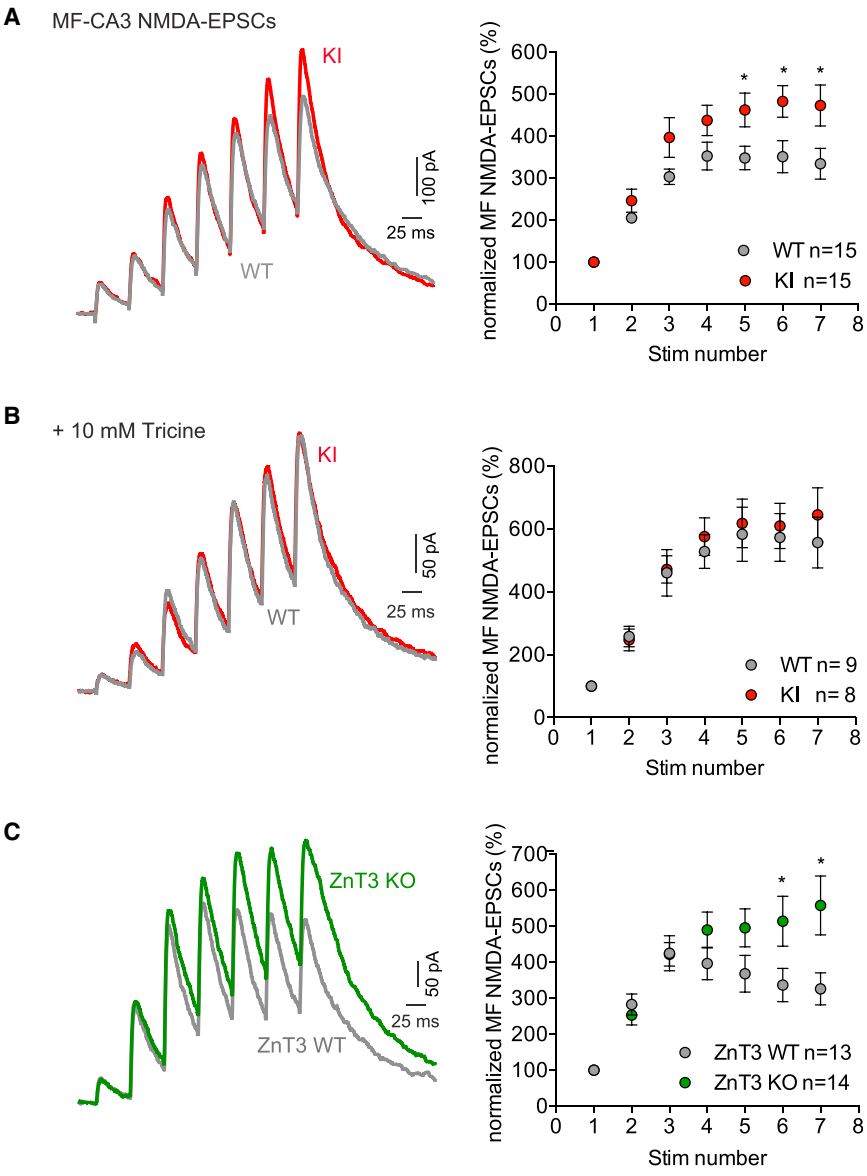

Figure 3. Burst-Induced Modulation of MF-CA3 NMDA-EPSCs by Vesicular Zinc

(A) Stimulating MFs with a short train consisting of seven stimuli at 25 Hz induced a significantly higher potentiation of MF-CA3 NMDA-EPSCs in KI than WT slices. Note that this difference appears only after the fourth pulse.

(B) In the presence of the zinc chelator tricine (10 mM), MF-CA3 NMDA-EPSCs from WT and KI mice were potentiated to the same extent.

(C) The same burst of MF stimulation yielded significantly higher potentiation of MF-CA3 NMDA-EPSCs in slices from ZnT3 KO mice than WT littermates. Data were normalized to the amplitude of the first NMDA-EPSC of the burst and are presented as mean ± SEM. *$p < 0.05$, Mann-Whitney test. See also Figures S3 and S4.

difference between ZnT3 KO and respective WT were suppressed in tricine (ratio seventh/first of 489% ± 52% [n = 10] versus 535% ± 82% [n = 7], respectively). These results confirm that zinc stored within vesicles of MF terminals provides the source of extracellular zinc-inhibiting MF-CA3 NMDA-EPSCs in an activity-dependent manner. No difference between ZnT3 KO and littermate WT controls was observed while recording AMPA-EPSCs (Figure S4B), ruling out that presynaptic effects of vesicular zinc account for the difference observed in NMDAR activity. Finally, in GluN2A KO slices, trains of NMDA-EPSCs, predominantly carried by GluN2B-receptors (Sakimura et al., 1995), were unaffected by zinc chelation (Figure S4E).

Collectively, these results indicate that a short burst of closely spaced action potentials is sufficient, but also necessary, for zinc action at MF-CA3 synapses. They also indicate that the high-affinity GluN2A zinc-binding site is a primary target of vesicular zinc and that zinc concentrations in the synaptic cleft are unlikely to impact on the macromolar binding sites of NMDARs. Zinc can thus act in a phasic fashion at MF-CA3 synapses. However, because several closely spaced release events are required for the zinc modulation to occur, a tonic-like mode of action in which zinc accumulates (build-up) in the large and tortuous synaptic cleft of MF-CA3 synapses may also be in play (see below). In order to estimate the duration during which zinc rise in the synaptic cleft may affect NMDA-EPSCs, we increased the rate of MF stimulation from 0.1 Hz to 1 or 3 Hz. We did not observe any difference between WT and KI in the relative amplitudes of MF-CA3 NMDA-EPSCs between 1 and 0.1 Hz (WT, 411% ± 24% [n = 15]; KI, 385% ± 21% [n = 15]) and between 3 and 0.1 Hz (WT, 770% ± 61% [n = 15]; KI, 697% ± 50% [n = 15]). This indicates that after a single synaptic event, zinc concentrations in the synaptic cleft return to basal levels, i.e., below low nanomolar levels, within a few hundred milliseconds.

Zinc Release and Modulation of NMDA-EPSCs at SC-CA1 Synapses

The hippocampal stratum radiatum displays significant staining for chelatable zinc (Sindreu et al., 2003), albeit at lower levels than the MF-containing stratum lucidum (Frederickson et al., 2000; Wenzel et al., 1997). Nonetheless, zinc release and action at the prototypical SC-CA1 glutamatergic synapses have attracted little attention in past studies.

We found no potentiating effect of the rapid-acting zinc chelator tricine during single synaptic events at SC-CA1 synapses in normal Mg^{2+} conditions (Figures S2D and S2E). Moreover, we observed no differential sensitivity of NMDA-EPSCs to tricine between WT and KI animals (Figures S2D and S2E). Hence, a

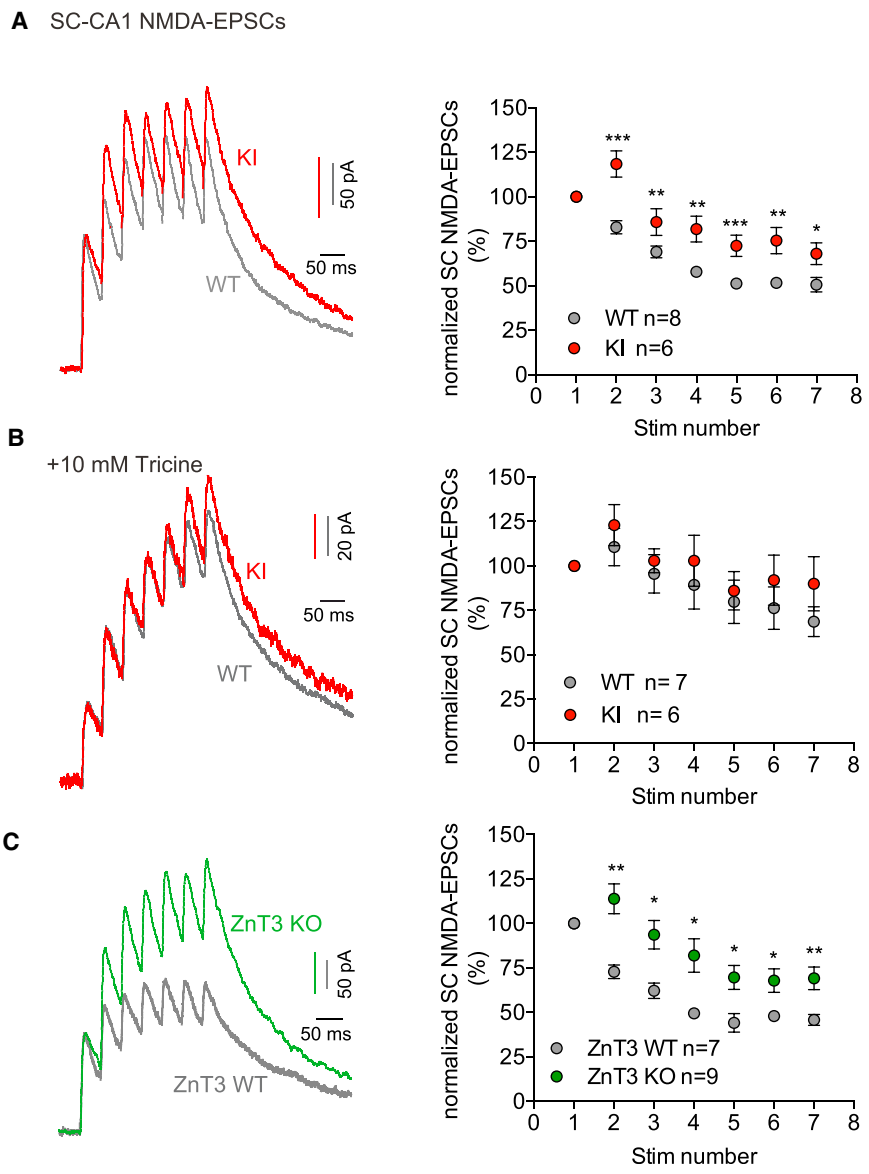

Figure 4. Burst-Induced Modulation of SC-CA1 NMDA-EPSCs by Vesicular Zinc

(A) Stimulating SC with a short train consisting of seven stimuli at 25 Hz induced a significantly higher potentiation of SC-CA1 NMDA-EPSCs in KI than WT slices. Note that this difference appears as soon as the second pulse.

(B) In the presence of the zinc chelator tricine (10 mM), MF-CA3 NMDA-EPSCs from WT and KI mice were potentiated to the same extent.

(C) The same burst of SC stimulation yielded significantly higher potentiation of SC-CA1 NMDA-EPSCs in slices from ZnT3 KO mice than WT littermates. Data were normalized to the amplitude of the first NMDA-EPSC of the burst and are presented as mean ± SEM. *p < 0.05, **p < 0.01, ***p < 0.001, Mann-Whitney test. See also Figures S3 and S4.

single synaptic event at SC-CA1 synapses appears insufficient to trigger zinc modulation of postsynaptic NMDARs, similarly to MF-CA3 synapses. We next explored whether repetitive stimuli at SC-CA1 synapses could result in detectable zinc elevations in the synaptic cleft. We again used the zinc sensitivity of NMDA-EPSCs as a functional readout of zinc availability in the vicinity of the postsynaptic membrane. NMDA-EPSCs evoked by two consecutive pulses at 1 or 3 Hz did not differ between WT and KI (second/first NMDA-EPSC ratio at 1 Hz: WT, 100% ± 2%, [n = 4]; KI, 95% ± 1%, [n = 8]; 3 Hz: WT, 86% ± 2% [n = 15]; KI, 91% ± 3%, [n = 12]). In contrast, comparing the evolution of NMDA-EPSC amplitudes during short trains of seven pulses at 25 Hz between WT, GluN2A-H128S KI, and ZnT3 KO animals revealed striking phenotypes. A pronounced difference between KI and WT was evident as early as the second pulse (Figure 4A). While in WT slices the amplitude of the second pulse was smaller than the amplitude of the first, in KI slices, the second pulse was systematically larger (ratio second/first of 122% ± 9% [n = 8] versus 83% ± 4% [n = 6] in WT). Furthermore, the KI/WT ratio in the NMDAR current amplitude reached its maximum at the second synaptic event and remained largely unchanged afterward, contrasting with the progressive increase at MF-CA3 synapses. In the presence of tricine, the differences between KI and WT NMDAR currents were suppressed (Figure 4B). By recording AMPA-EPSCs, we also verified that KI and WT mice did not differ in SC-CA1 short-term plasticity (Figure S4C). These results show that a pair of consecutive and closely spaced synaptic discharges in SCs is sufficient to induce zinc modulation of CA1 NMDARs. In slices from ZnT3 KO mice, the mean behavior of NMDA-EPSCs in response to 25 Hz burst stimulation of SCs differed from WT littermates and was strikingly similar to that observed with KI animals (Figure 4C), indicative of the vesicular origin of zinc acting at postsynaptic NMDARs. The difference between ZnT3 KO and littermate WT animals was specific to NMDAR responses, since no difference was detected for AMPA-EPSCs between the two genotypes (Figure S4D). Finally, in GluN2A KO slices, tricine had no effect on SC-CA1 NMDA-EPSCs (Figure S4F).

Altogether, these results indicate that closely spaced repetitive stimuli of SCs elicit vesicular zinc release and the ensuing modulation of postsynaptic CA1 NMDARs. They also reveal that zinc selectively occupies high-affinity GluN2A inhibitory sites.

Modulation of NMDAR-Dependent Synaptic Integration and Plasticity by Vesicular Zinc

Because vesicular zinc modulates synaptic function by acting on postsynaptic NMDARs in a use-dependent manner, we next

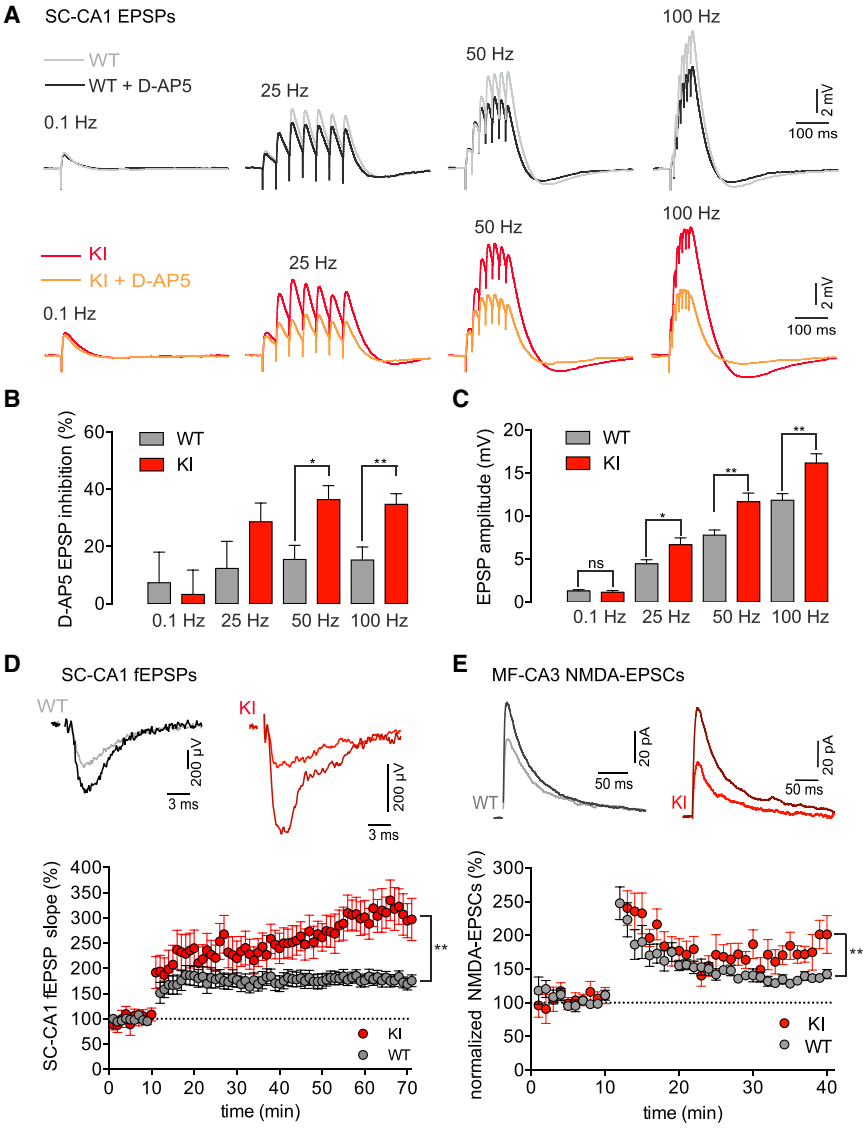

Figure 5. Zinc Contribution to Synaptic Integration and Plasticity at SC-CA1 Synapses

(A) Representative traces illustrating the impact of D-AP5 application on SC-CA1 EPSPs elicited using a single stimulation at 0.1 Hz or a train of seven stimulations at 25, 50, and 100 Hz, in WT and KI mice.

(B) Summary plot of D-AP5 effect on SC-CA1 EPSP amplitude in WT and KI mice. Note the larger contribution of NMDARs in KI than WT mice at high frequencies of stimulation.

(C) Averaged SC-CA1 EPSP amplitudes in WT and KI mice. During train protocols, EPSP amplitudes were significantly greater in KI than WT slices.

(D) Enhanced SC-CA1 LTP in KI mice. Top: representative traces of fEPSPs before and after LTP induction in WT and KI slices. Bottom: normalized fEPSP slope before and after LTP induction (at 10 min).

(E) Enhanced MF-CA3 LTP_{NMDA} in KI mice. Top: representative traces of MF-CA3 NMDA-EPSCs before and after plasticity induction in WT and KI slices. Bottom: normalized NMDA-EPSC amplitude before and after LTP induction (at 10 min). Data are presented as mean ± SEM. *p < 0.05, **p < 0.01, Mann-Whitney test for (B), (D), and (E). *p < 0.05, **p < 0.01 Student's unpaired t test for (C). See also Figure S5.

investigated the impact of endogenous zinc on NMDAR-dependent synaptic integration and plasticity. The slow deactivation kinetics of NMDARs and their unique voltage dependence endowed by the Mg^{2+} block allow for robust temporal summation and nonlinear amplification of synaptic inputs (Hunt and Castillo, 2012). To evaluate the possible modulation of synaptic integration by vesicular zinc through modulation of postsynaptic NMDARs, we compared the participation of NMDARs to individual SC-CA1 excitatory postsynaptic potentials (EPSPs) (0.1 Hz) and after trains of stimulations (seven stimuli at 25, 50, and 100 Hz) between WT and KI mice. D-AP5 applications revealed that NMDARs do not participate significantly to the amplitude of individual EPSPs in both genotypes (WT: 98% ± 11% [n = 8]; KI: 97% ± 9% [n = 7]; Figures 5A and 5B). In contrast, during train protocols, NMDARs contributed to EPSP amplitude, probably reflecting decreased Mg^{2+} block due to increased EPSP amplitude. Remarkably, the contribution of NMDARs to the EPSPs was larger in KI than WT mice (Figures 5A and 5B), suggesting that zinc release at SC-CA1 synapses during repetitive stimulations reduces EPSP amplitude by limiting NMDAR activity. In agreement, trains of stimulation induced significantly higher level of depolarization in KI than WT mice (Figure 5C). This difference was abolished in the presence of D-AP5 and did not result from differences in resting membrane potential or input resistance between WT and KI CA1 pyramidal cells (Figures S5A and 5B).

At SC-CA1 synapses, NMDAR-dependent long-term plasticity can be triggered by high-frequency or theta-burst stimulation (Malenka and Bear, 2004), conditions that should be favorable for elevating synaptic zinc levels. We first induced long-term potentiation (LTP) at SC-CA1 synapses by tetanic stimulation of SCs while recording fEPSPs in the stratum radiatum. This protocol yielded a long-lasting increase in the fEPSP slope in both WT and KI but the effect was much larger in KI slices (310% ± 36% [n = 10] versus 169% ± 12% [n = 10] for WT; Figure 5D). Facilitated LTP was also obtained when using a theta-burst protocol (277% ± 37% [n = 6] for KI versus 165% ± 13% [n = 6] for WT; Figure S5C). Hence, zinc release by trains of stimulation acts as a negative regulator of SC-CA1 LTP by selectively silencing GluN2A-NMDARs. MF-CA3 synapses do not express the classical postsynaptic NMDAR-dependent plasticity but display a NMDAR-dependent LTP of NMDA-EPSCs (LTP_{NMDA}; Kwon and Castillo, 2008; Rebola et al., 2008). Using short bursts of seven stimuli at 25 Hz separated by 140 ms to trigger

LTP_{NMDA} (Rebola et al., 2008), we found that the magnitude of LTP_{NMDA} was markedly increased in KI mice compared to WT mice (175% ± 15% [n = 8] increase of NMDA-EPSCs 30–40 min after the bursts in KI slices versus 135% ± 3% [n = 12] in WT; Figure 5E). The disrupted GluN2A-zinc interaction in KI mice thus unmasks a potent inhibitory action of endogenous zinc on MF-CA3 LTP_{NMDA} by dampening activity of GluN2A-containing NMDARs.

Quantifying Zinc Dynamics and Receptor Actions at MF-CA3 and SC-CA1 Synapses

To obtain a quantitative framework pertinent to zinc release, diffusion, and NMDAR activation inside the synaptic cleft, we turned to computational modeling. We took advantage of previously established Monte Carlo models (Savtchenko et al., 2013; Sylantyev et al., 2008), adapting them to mimic the microenvironment of MF-CA3 and SC-CA1 synapses, two synapses that differ strikingly, both anatomically and functionally.

While the modeled representation of small, single-release site SC-CA1 synapses has been extensively validated (Savtchenko et al., 2013; Sylantyev et al., 2008), we carried out a separate study to construct a computationally viable and representative geometry of complex synapses formed by MFs on thorny excrescences of CA3 pyramid cells. In brief, the model was based on the parameters of "average" MF-CA3 geometry reported by comprehensive 3D EM reconstructions (Rollenhagen et al., 2007). This included 12 main (plus several truncated) protrusions (each hosting a release site), the total surface area of ~60 μm^2, the pre-/postsynaptic interface (cleft) area of ~30 μm^2, and the overall caliper of 3–4 μm (Figure 6A; see Experimental Procedures). The model recapitulates stochastic release of glutamate and zinc from multiple release sites, Brownian diffusion of individual glutamate molecules and zinc ions inside the tortuous synaptic cleft (Figure 6B), and full GluN2A-NMDAR kinetics incorporating the zinc-binding steps (Erreger and Traynelis, 2005). To account for the removal of extracellular zinc (Sensi et al., 2009), the model incorporated simple zinc uptake kinetics, with a removal rate of 30 ms^{-1} as reported previously in hippocampal slices (Howell et al., 1984). GluN2A-NMDARs, which prevail at mature MF-CA3 synapses (Fritschy et al., 1998; Watanabe et al., 1998), were scattered within the postsynaptic densities (PSDs) facing individual active zones.

With the model parameters representing an average MF-CA3 synapse, simulated NMDAR currents readily replicated recorded NMDA-ESPCs (Figure 6C). To reproduce use-dependent facilitation of transmission at these synapses at 25 Hz (Figure 3), we had to set release probability at individual release sites (Pr) at the best-fit baseline value of ~0.02, which progressively increased to 0.04, 0.08, 0.12, 0.16, 0.2, and 0.25 for the train discharges (see Experimental Procedures). At the same time, we varied the amount of zinc coreleased with glutamate to find that the NMDAR-response time course observed in WT mice during the 25 Hz train protocol was best reproduced when the number of zinc ions per vesicle was one-twentieth of that of glutamate molecules (Figure 6D). The model also reproduced the key observation that a single corelease event of glutamate and zinc has little effect on postsynaptic NMDAR responses. In relation to the latter observation, simulations supported the hypothesis that the lack of zinc sensitivity for the first NMDAR response was due to the delayed onset of zinc action on NMDAR kinetics (compared to the fast NMDAR activation by glutamate). After the first synaptic event, however, zinc remains bound to GluN2A subunits for many tens of milliseconds (Figure 6E) owing to its slow dissociation (Erreger and Traynelis, 2005; Paoletti et al., 1997). Consequent to this, NMDAR activation is modulated upon subsequent glutamate release. Thus, zinc is likely to affect NMDARs at repeatedly activated synapses, as opposed to relatively silent ones. Inside large and tortuous synaptic clefts, such as that at MF-CA3 synapses, multiple release events will progressively increase the overall intracleft zinc concentration (because of the relatively slow diffusion escape), thus gradually boosting zinc effect on NMDARs. Finally, our model faithfully reproduced the lack of zinc effect on NMDA-EPSCs when stimulating MFs at 3 Hz (Figure S6), consistent with zinc dissociating from GluN2A-NMDARs and escaping the cleft within hundreds of milliseconds.

The model of SC-CA1 synapses (in which ~50% of NMDARs were assumed to be of the GluN1/GluN2A subtype; see Experimental Procedures) also captured most zinc-related features recorded at these synapses (Figures 6F–6J). This included the near-maximum inhibition effect by zinc seen already by the second synaptic event during the 25 Hz train stimulation. The model provides a straightforward mechanistic explanation for this phenomenon. In contrast to MF-CA3 synapses, single-site SC-CA1 synapses show a relatively high release probability. Indeed, the best-fit simulations corresponded to Pr = 0.3 in resting conditions, rising to Pr = 0.5 for the subsequent discharges in the stimulus train, concordant with experimental Pr and its use-dependent increases monitored directly at SC-CA1 synapses using optical quantal analyses (Oertner et al., 2002; Sylantyev et al., 2013). As for the zinc effect on NMDARs, the high Pr values imply that after one to two release events, the effect will be close to saturation because by the second discharge most GluN2A-NMDARs will already have had bound zinc. This is precisely what we observed in our experiments (Figure 4). Finally, our simulation indicated that the experimental data corresponded to a zinc content in a single SC vesicle around one-twentieth that of glutamate (Figure 6I), similar to synaptic vesicles at MF-CA3 synapses.

Zinc Action Is Highly Dependent on Release Probability

During our exploration of the synaptic models, Pr was found to be a critical parameter in determining the extent of zinc action at postsynaptic NMDARs. The very low basal Pr for individual release sites at MF-CA3 synapses makes the recruitment of the same sites very unlikely during early phases of train stimulations, thus explaining the substantial delay, and the progressive nature, of zinc action at MF-CA3 synapses, an effect absent at high Pr SC-CA1 synapses (compare Figures 3 and 4). Our model thus predicted that increasing basal Pr of MFs should induce a major change in the impact that vesicular zinc produces on the synaptic response (i.e., NMDA-EPSCs), in particular by allowing zinc to manifest its modulatory (inhibitory) effect early on during train protocols (Figure S7). Performing train experiments on MFs with enhanced basal Pr fully bore out this prediction. After conditioning MFs with 3 Hz stimuli to boost Pr, applying 25 Hz burst stimulations revealed a marked difference between WT and KI

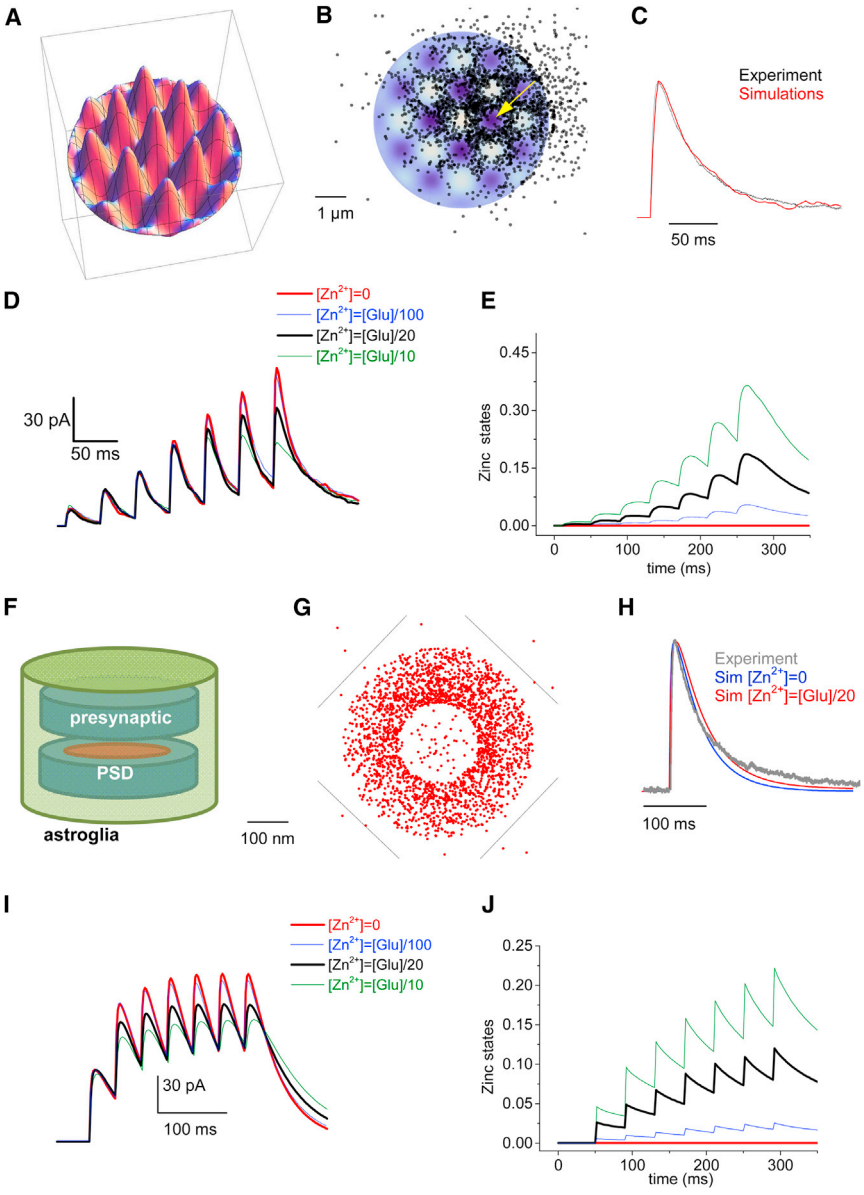

Figure 6. Monte Carlo Modeling of Zinc Diffusion and NMDAR Action at MF-CA3 and SC-CA1 Synapses

(A) A 3D schematic depicting the simulated interface of pre- and postsynaptic membranes of MF-CA3 synapses (thorny excrescences) that recapitulates average geometry quantified in a detailed 3D reconstruction study (Rollenhagen et al., 2007).

(B) A snapshot of diffusing glutamate molecules 2 ms after release of a single vesicle (2,500 molecules) from the site shown by the arrow; view from above as in (A).

(C) Characteristic traces of experimentally recorded (black) and simulated (red) MF-CA3 NMDA-EPSCs in response to single-vesicle release (as in B).

(D) Probing the role of zinc in shaping evoked NMDAR currents at MF-CA3 synapses. Characteristic average traces of NMDA-EPSCs recorded in a CA3 pyramidal cell in response to seven stimuli applied to MFs at 25 Hz for four different concentrations of zinc inside released vesicles, as indicated. Individual traces represent a 20-trial average (see Experimental Procedures for details).

(E) The dynamics of the zinc-dependent NMDAR states in simulations depicted in (D).

(F) A 3D schematic depicting the simulated interface of pre- and postsynaptic membranes of CA1 synapses.

(G) A snapshot of diffusing glutamate molecules 1 ms after release of a single vesicle (2,500 molecules).

(H) Characteristic average traces of experimentally recorded (gray) and simulated (blue and red; two selected zinc concentration inside synaptic vesicles, as indicated) SC-CA1 NMDA-EPSCs in response to a single stimulus applied to SC.

(I) Probing the role of zinc in shaping evoked NMDAR currents at CA3-CA1 synapses. Simulated NMDA-EPSCs traces, in conditions replicating experiments in which seven stimuli were applied to SC at 25 Hz, for four different concentrations of zinc inside released vesicles, as indicated.

(J) The dynamics of zinc-dependent NMDAR states in simulations depicted in (I). See also Figure S6 for Monte Carlo simulations at low-frequency stimulation.

NMDA-EPSCs as soon as the third pulse in the burst, and this difference remained constant until the last (seventh) pulse (Figure 7). In such conditions, the overall pattern of MF-CA3 NMDA-EPSCs during the burst stimulations appeared transformed compared to the situation observed with nonconditioned low Pr MFs (compare Figures 7B and 7C and 3A). In fact, this transformed MF-CA3 pattern showed obvious similarities with that previously observed at SC-CA1 synapses, indicating similar zinc temporal profile and action between the two synapses (compare Figures 7B and 7C and 4A). Overall, these results reveal a major influence of Pr on zinc action at excitatory synapses. Hence, at a given synapse, the dynamics and physiological actions of zinc are not fixed but depend on preceding activity, i.e., "synapse history."

DISCUSSION

The presence of high levels of zinc in synaptic vesicles within the mammalian forebrain has intrigued neuroscientists for decades. An unresolved yet central issue relates to zinc levels and dynamics within the synaptic cleft both under basal conditions and following neuronal activity. Here, using a combination of genetic tools, fast chelating agent, and modeling approaches, we decrypt the spatiotemporal zinc profile at excitatory synapses and reveal that endogenous zinc contained in synaptic vesicles is a potent neuromodulator that shapes NMDAR-mediated responses by specifically acting on the nanomolar GluN2A binding site. Zinc action is highly dependent on the pattern of presynaptic activity and release probability. Moreover, in contrast to the

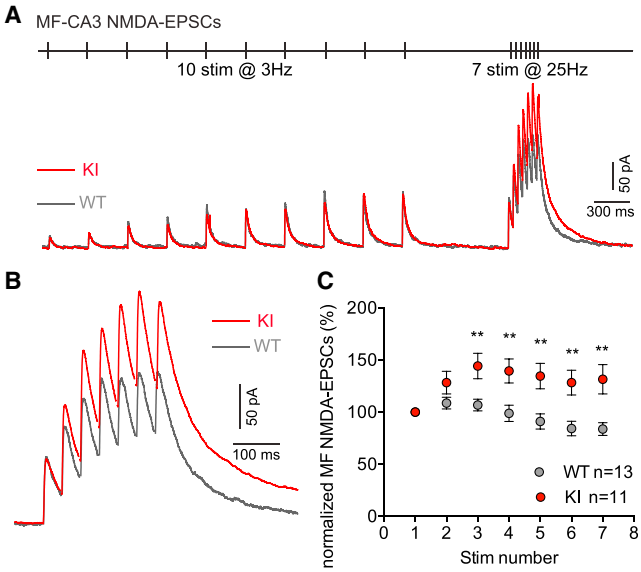

Figure 7. Increasing Release Probability at MF-CA3 Synapses Facilitates Zinc Modulation of NMDARs

(A) The probability of release at mossy fiber synapses was increased by applying a conditioning stimulus (ten stimulations at 3 Hz) prior to burst stimulation (seven stimuli at 25 Hz).

(B) After the conditioning stimulus, burst stimulation induced significantly higher potentiation of NMDA-EPSCs in KI versus WT slices. Note that under these conditions, zinc modulation was detected as soon as the third pulse and remained constant throughout the following pulses, a pattern resembling that obtained at SC-CA1 synapses (see Figure 4A).

(C) Data were normalized to the amplitude of the first NMDA-EPSC in the burst and are presented as mean ± SEM. **$p < 0.01$, Mann-Whitney test. See also Figure S7 for Monte Carlo simulations of zinc action on NMDARs at MF-CA3 synapses with increased release probability.

common belief, we show that zinc action is not restricted to hippocampal MFs but extends to SC-CA1 excitatory synapses, where it controls synaptic integration and plasticity. This probably applies to all other zinc-positive synapses in the brain. Hence, by providing a description of synaptic zinc dynamics with unprecedented accuracy and resolution, our work lays the foundation for a comprehensive understanding of zinc action in neural circuits.

To gain access to the levels of synaptic zinc, we utilized GluN2A-H128S KI mice, in which the high-affinity (nanomolar) GluN2A-NMDAR zinc inhibitory site has been selectively eliminated (Nozaki et al., 2011). Comparing NMDAR-mediated synaptic responses between WT and KI mice allowed us to evaluate the levels of zinc in the synaptic cleft under various conditions of neuronal activity. In contrast to studies using zinc dyes homogenously distributed within the slice (Komatsu et al., 2005; Li et al., 2001; Nydegger et al., 2010; Qian and Noebels, 2005, 2006; Ueno et al., 2002), our approach relying on single-cell EPSC measurements informs on the zinc levels at the strategic location in the very vicinity of the postsynaptic receptors. We first demonstrate that in resting conditions, ambient synaptic zinc levels are extremely low (<10 nM) even at MF-CA3 synapses, the most zinc-enriched synapses within the brain. This contrasts with previous data suggesting that ambient zinc levels at MF-CA3 synapses are high enough to tonically occupy (and saturate) the nanomoloar zinc sites on NMDARs (Vogt et al., 2000). We explain this apparent discrepancy by showing that lowering extracellular Mg^{2+} concentrations, as done by Vogt and colleagues, artificially increases extracellular zinc levels through enhanced exocytosis of vesicular zinc. It will then be interesting to investigate whether ambient zinc levels are elevated in physiopathological conditions associated with overexcitability (e.g., status epilepticus). Given that zinc is present endogenously in the cerebrospinal fluid (at a "free" concentration of ~20 nM [Frederickson et al., 2006b; Sindreu and Storm, 2011]) and as a contaminant in recording (i.e., ACSF) solutions at a concentration (~200 nM; P.P., unpublished data) well above the zinc IC_{50} for high-affinity GluN2A sites, the complete absence of tonic GluN2A-NMDAR inhibition by ambient zinc in normal magnesium conditions points to the existence of a powerful zinc uptake mechanism regulating the availability of zinc in the synaptic cleft. Several mechanisms of zinc influx at the neuronal plasma membrane have been described (Sensi et al., 2009), including zinc uptake by members of Zip transporters family such as Zip-1 and Zip-3, which show strong expression in the hippocampus (Qian et al., 2011). The functional relevance of Zip proteins and other potential zinc clearance mechanisms in controlling zinc levels in the synaptic cleft is yet to be established, a task made difficult by the lack of appropriate pharmacological tools.

We show that following neuronal activity, vesicular zinc is coreleased with glutamate in the synaptic cleft and diffuses to the postsynaptic membrane, where it binds to GluN2A-NMDARs. Zinc increases transiently in the synaptic cleft, where it has a short lifetime (<2 ms at SC-CA1 synapse; <30–40 ms at MF-CA3 synapses; Figure S6) and reaches concentrations sufficient to occupy the high-affinity (nanomolar), but not the low affinity (micromolar), zinc sites on postsynaptic receptors. Using Monte Carlo simulations, we calculated that ~125 zinc ions populate a single MF or SC vesicle corresponding to a luminal vesicular concentration of 1–5 mM, in good agreement with previous estimations (Frederickson et al., 2000; Sindreu and Storm, 2011). The actual number may be slightly higher though since in our model we assumed all synaptic vesicles to contain zinc, which is still a matter of debate (Lavoie et al., 2011; Sindreu et al., 2003; Wenzel et al., 1997). It remains that the vesicular zinc content appears significantly lesser than that of glutamate (20–100 mM), arguing for tightly time- and space-controlled zinc action(s) in the synaptic cleft following its release.

By quantifying the extracellular zinc profile at excitatory synapses, our work settles the lingering issue of zinc concentrations and dynamics in the synaptic cleft that has opposed extreme views for years—from no (Kay, 2003; Kay and Tóth, 2008; Nydegger et al., 2010) to massive (Besser et al., 2009; Frederickson et al., 2006a; Li et al., 2001; Molnár and Nadler, 2001; Ueno et al., 2002; Vogt et al., 2000) zinc release. Elucidation of the exact zinc dynamics at excitatory synapses has major implications in identifying possible targets of synaptically released zinc. Thus, synaptic proteins with low (>10 μM) zinc sensitivity such as AMPA receptors and glutamate transporters are unlikely to serve as zinc targets, at least in physiological conditions. In agreement, we observed no effect of vesicular zinc on AMPA-EPSCs during train protocols (Figure S4). The question also arises whether the

recently described putative metabotropic zinc-binding receptor (mZnR; also known as GPR39) is a bona fide zinc "sensor" in normal conditions given its low zinc affinity (K_d ~150 μM [Besser et al., 2009; Perez-Rosello et al., 2013]). In contrast, NMDARs that harbor a GluN2A-specific nanomolar zinc site appear obvious candidates for zinc binding, and our current work reveals that GluN2A-NMDARs, but not the less zinc-sensitive GluN2B-NMDARs, are indeed major targets of vesicular zinc. We predict that ASIC1 channels, which also contain a low nanomolar zinc inhibitory site (Chu et al., 2004) and cluster at the PSD (Wemmie et al., 2002), may also be modulated by endogenous synaptic zinc. The case of the inhibitory GABA-A and glycine receptors, which display a wide range of zinc sensitivity depending on subunit composition (from low nanomolar to high micromolar [Hosie et al., 2003; Smart et al., 2004]), appears more intriguing given that zinc-positive synapses in the brain are almost exclusively glutamatergic (Frederickson et al., 2000). Zinc spillover from excitatory to inhibitory synapses may allow zinc modulation of postsynaptic GABAergic receptors (Kodirov et al., 2006), although how much zinc can reach inhibitory synapses once its escapes from neighboring excitatory synapses is unclear.

By monitoring NMDAR-mediated responses at hippocampal SC-CA1 and MF-CA3 synapses, we provide direct evidence that zinc is a powerful activity-dependent modulator of excitatory neurotransmission. We establish that zinc action depends in a rather unique way on release probability and on the pattern of presynaptic activity. Indeed, following a single synaptic release event, the zinc coreleased with glutamate is functionally "silent." Zinc action at postsynaptic NMDARs requires trains of closely spaced synaptic release events (at the very same active zone). This behavior departs from that of classical fast neurotransmitters, for which each individual release event usually triggers a detectable postsynaptic response. This requirement for repetitive activity finds its origin in the slow zinc kinetics on GluN2A-NMDARs. During a single synaptic discharge, the zinc coreleased with glutamate binds postsynaptic GluN2A-NMDARs, but re-equilibration to zinc-inhibited receptor states is slow (compared to glutamate activation; Erreger and Traynelis, 2005), thus explaining the insensitivity of individual synaptic currents to vesicular zinc. However, once bound to GluN2A sites, zinc dissociates slowly such that any glutamate release event that occurs within <300 ms from a preceding release event will be affected. As a consequence, and as predicted by our Monte Carlo simulations, zinc action on NMDARs is expected to be stronger at synaptic sites that experience multiple release events close in time than at sites with sparse activity. Hence, zinc action required both high Pr and repetitive presynaptic activity. In agreement, we experimentally show that vesicular zinc release significantly limits the participation of NMDARs to SC-CA1 EPSPs upon trains of synaptic stimulation, while not affecting single EPSPs. The critical role of basal Pr in controlling the extent of zinc action was also confirmed by recordings from MF-CA3 synapses with differing levels of Pr.

The discovery that zinc acts as a use-dependent synaptic modulator and selectively modulates GluN2A-NMDARs has wide-ranging implications for neuronal computation. It is thus expected that vesicular zinc will be most effective during burst activity and thus impact NMDAR-controlled integration time window, which is critical in recognizing and subsequently generating bursts of action potential (Hunt and Castillo, 2012). Similarly, we anticipate plasticity based on induction protocols using low-frequency presynaptic stimulation (like spike-timing-dependent plasticity) to be zinc insensitive in contrast to plasticity induced by high-frequency or theta-burst stimulations (as shown in Figures 5 and S5). Hence, zinc endows neurons with the ability to discriminate between various types of plasticity induction. Moreover, zinc by selectively inhibiting GluN2A-NMDARs is expected to favor GluN2B signaling with major consequences on subsequent plasticities (metaplasticity; Paoletti et al., 2013).

Is there a potential benefit of the coexistence in the mammalian brain of zinc-positive and zinc-negative glutamatergic fibers? Noticeably, the same neuronal population can be contacted by both types of fibers (e.g., zinc-positive SCs versus zinc-negative temporoammonic terminals on CA1 pyramidal cells [Frederickson et al., 2000; Sindreu et al., 2003]). Our data suggest that zinc-positive and zinc-negative fibers impart differential synaptic integration and plasticity rules onto the same neuron. Recent evidence uncovering specific cognitive deficits in ZnT3 KO mice (Adlard et al., 2010; Martel et al., 2010, 2011; Sindreu et al., 2011) hints to important physiological roles of vesicular zinc, but the cellular and network correlates of these behavioral alterations remain unclear. Similarly, the excessive accumulation of zinc at excitatory synapses in Alzheimer's disease (Sensi et al., 2011) together with the recent identification of a mutation in the *Grin2A* gene causing impaired GluN2A-zinc interaction in children with idiopathic focal epilepsy (Lemke et al., 2013) strongly support a critical role of synaptic zinc in human health. By deciphering zinc dynamics in the synaptic cleft and its impact on glutamate receptors, our current work provides the long-awaited framework necessary to understand how zinc may contribute to the functional diversity of excitatory synapses and more generally to brain function and dysfunction.

EXPERIMENTAL PROCEDURES

All experiments were performed in accordance with the European Communities Council Directive of 24 November 1986 and the European Directive 2010/63/EU on the Protection of Animals used for Scientific Purposes.

Slice Electrophysiology

Hippocampal transverse (320-μm-thick, CA1 experiments) or parasagittal (350-μm-thick, CA3 experiments) slices were obtained from 3- to 4-week-old mice killed by cervical dislocation or by decapitation following deep pentobarbital anesthesia (30 mg/kg). Slices were transferred to a recording chamber perfused with a bubbled (95% O_2 and 5% CO_2) artificial cerebrospinal fluid (ACSF) typically containing 125 mM NaCl, 2.5 mM KCl, 2 (CA1) or 2.3 mM (CA3) $CaCl_2$, 1 mM (CA1) or 1.3 mM (CA3) $MgCl_2$, 1.25 mM NaH_2PO_4, 26 mM $NaHCO_3$, 20 mM glucose, and 0.01 mM bicuculline. Mg^{2+} concentrations were higher in CA3 experiments to minimize CA3 excitability and improve the quality of MF-CA3 recordings. In some experiments, Mg^{2+} concentrations were reduced to 0.3 mM or 0 (i.e., no added Mg^{2+}) while maintaining the Ca^{2+}/Mg^{2+} ratio by increasing Ca^{2+} concentrations accordingly.

For voltage-clamp recordings in normal extracellular magnesium, patch pipettes were filled with an intracellular solution containing 125 mM Cs-gluconate or methanesulfonate, 20 mM BAPTA, 5 mM QX-314, 5 mM TEA-Cl, 10 mM HEPES, 4 mM ATP-Mg, and 0.2 mM GTP-Na (pH 7.3 with CsOH).

For recordings in low extracellular magnesium, the patch pipettes were filled with a solution containing 145 mM Cs-gluconate, 0.2 mM EGTA, 5 mM QX-314, 5 mM TEA-Cl, 10 mM HEPES, and 4 mM ATP-Mg (pH 7.3 with CsOH). Current-clamp recordings were performed in 1.0 mM Mg^{2+} using the following intracellular solution: 145 mM K-gluconate, 0.2 mM EGTA, 10 mM HEPES, and 4 mM ATP-Mg (pH 7.3 with KOH). Further information regarding electrophysiological procedures is provided in the Supplemental Experimental Procedures.

Synaptic Modeling

Monte Carlo models adapted to mimic the microenvironment of MF-CA3 and SC-CA1 synapses were applied. The modeled structure of MF-CA3 synapses was based on the recent quantitative morphological study (Rollenhagen et al., 2007). In the model of SC-CA1 hippocampal synapses, the methodology and algorithms were adapted from previous approaches (Savtchenko et al., 2013; Sylantyev et al., 2008). The models recapitulate stochastic release of glutamate and zinc (from multiple release sites in the case of MF-CA3 synapses), Brownian diffusion of individual glutamate molecules and zinc ions inside the synaptic cleft and full GluN2A-NMDAR kinetics incorporating the zinc-binding steps (Erreger and Traynelis, 2005). Detailed information regarding synaptic modeling is provided in the Supplemental Experimental Procedures.

Data Analysis

Data were analyzed using IGOR Pro or NeuroMatic (http://www.neuromatic.thinkrandom.com) within the IGOR Pro environment (WaveMetrics). Results are expressed as mean ± SEM, unless otherwise indicated; n indicates the number of different cells. Statistical comparisons were performed using Student's t test and statistical significance was set at 0.05. Statistical comparison between normalized data was performed using nonparametric Mann-Whitney test. EPSP amplitudes during trains of stimulation were obtained by measuring the maximal amplitude value reached during the train of EPSPs. For LTP experiments and experiments on zinc chelator effects on NMDA-EPSCs, statistical significance was assessed by averaging the last 10 min of recording in each condition and applying a nonparametric Mann-Whitney test on these values.

SUPPLEMENTAL INFORMATION

Supplemental Information includes Supplemental Experimental Procedures and seven figures and can be found with this article online at http://dx.doi.org/10.1016/j.neuron.2014.04.034.

AUTHOR CONTRIBUTIONS

C.M. and P.P. designed and supervised the study. B.L.K contributed to the generation of the GluN2A-H128S mutant mouse line. A.M.V. and N.R. performed all the electrophysiological recordings. P.S.P. and M.C. helped with the initial characterization of MF-CA3 and SC-CA1 GluN2A-H128S KI synaptic properties, respectively. L.P.S. and D.A.R. conceived and performed synaptic modeling studies. A.M.V, N.R., L.P.S, D.A.R. C.M., and P.P. wrote the manuscript.

ACKNOWLEDGMENTS

This work was supported by Agence Nationale de le Recherche (ANR grants to C.M. and P.P.), Fondation pour la Recherche Médicale ('Equipe FRM' grant DEQ2000326520 to P.P.) and Région Ile-de-France (A.M.V.); Wellcome Trust Principal Fellowship, European Research Council Advanced Grant, BBSRC, and EU BM1001 Cost Action (D.A.R.). This work also received support from the French government under the program "Investissements d'Avenir" (ANR-10-LABX-54 MEMO LIFE and ANR-11-IDEX-0001-02 PSL* Research University). We are grateful to Steven Traynelis for help with the NMDAR kinetic scheme and Kaiyu Zheng for help with computational cluster environment.

Accepted: April 15, 2014
Published: June 4, 2014

REFERENCES

Adlard, P.A., Parncutt, J.M., Finkelstein, D.I., and Bush, A.I. (2010). Cognitive loss in zinc transporter-3 knock-out mice: a phenocopy for the synaptic and memory deficits of Alzheimer's disease? J. Neurosci. *30*, 1631–1636.

Aniksztejn, L., Charton, G., and Ben-Ari, Y. (1987). Selective release of endogenous zinc from the hippocampal mossy fibers in situ. Brain Res. *404*, 58–64.

Assaf, S.Y., and Chung, S.H. (1984). Release of endogenous Zn2+ from brain tissue during activity. Nature *308*, 734–736.

Besser, L., Chorin, E., Sekler, I., Silverman, W.F., Atkin, S., Russell, J.T., and Hershfinkel, M. (2009). Synaptically released zinc triggers metabotropic signaling via a zinc-sensing receptor in the hippocampus. J. Neurosci. *29*, 2890–2901.

Carter, R.E., Aiba, I., Dietz, R.M., Sheline, C.T., and Shuttleworth, C.W. (2011). Spreading depression and related events are significant sources of neuronal Zn2+ release and accumulation. J. Cereb. Blood Flow Metab. *31*, 1073–1084.

Chen, N., Moshaver, A., and Raymond, L.A. (1997). Differential sensitivity of recombinant N-methyl-D-aspartate receptor subtypes to zinc inhibition. Mol. Pharmacol. *51*, 1015–1023.

Choi, Y.B., and Lipton, S.A. (1999). Identification and mechanism of action of two histidine residues underlying high-affinity Zn2+ inhibition of the NMDA receptor. Neuron *23*, 171–180.

Chu, X.P., Wemmie, J.A., Wang, W.Z., Zhu, X.M., Saugstad, J.A., Price, M.P., Simon, R.P., and Xiong, Z.G. (2004). Subunit-dependent high-affinity zinc inhibition of acid-sensing ion channels. J. Neurosci. *24*, 8678–8689.

Cole, T.B., Wenzel, H.J., Kafer, K.E., Schwartzkroin, P.A., and Palmiter, R.D. (1999). Elimination of zinc from synaptic vesicles in the intact mouse brain by disruption of the ZnT3 gene. Proc. Natl. Acad. Sci. USA *96*, 1716–1721.

Erreger, K., and Traynelis, S.F. (2005). Allosteric interaction between zinc and glutamate binding domains on NR2A causes desensitization of NMDA receptors. J. Physiol. *569*, 381–393.

Fayyazuddin, A., Villarroel, A., Le Goff, A., Lerma, J., and Neyton, J. (2000). Four residues of the extracellular N-terminal domain of the NR2A subunit control high-affinity Zn^{2+} binding to NMDA receptors. Neuron *25*, 683–694.

Frederickson, C.J., Suh, S.W., Silva, D., Frederickson, C.J., and Thompson, R.B. (2000). Importance of zinc in the central nervous system: the zinc-containing neuron. J. Nutr. Suppl. *130*, 1471S–1483S.

Frederickson, C.J., Giblin, L.J., 3rd, Balaji, R.V., Masalha, R., Frederickson, C.J., Zeng, Y., Lopez, E.V., Koh, J.Y., Chorin, U., Besser, L., et al. (2006a). Synaptic release of zinc from brain slices: factors governing release, imaging, and accurate calculation of concentration. J. Neurosci. Methods *154*, 19–29.

Frederickson, C.J., Giblin, L.J., Krezel, A., McAdoo, D.J., Mueller, R.N., Zeng, Y., Balaji, R.V., Masalha, R., Thompson, R.B., Fierke, C.A., et al. (2006b). Concentrations of extracellular free zinc (pZn)e in the central nervous system during simple anesthetization, ischemia and reperfusion. Exp. Neurol. *198*, 285–293.

Fritschy, J.M., Weinmann, O., Wenzel, A., and Benke, D. (1998). Synapse-specific localization of NMDA and GABA(A) receptor subunits revealed by antigen-retrieval immunohistochemistry. J. Comp. Neurol. *390*, 194–210.

Gielen, M., Le Goff, A., Stroebel, D., Johnson, J.W., Neyton, J., and Paoletti, P. (2008). Structural rearrangements of NR1/NR2A NMDA receptors during allosteric inhibition. Neuron *57*, 80–93.

Grauert, A., Engel, D.A., and Ruiz, A.J. (2014). Endogenous zinc depresses GABAergic transmission via T-type Ca(2+) channels and broadens the time window for integration of glutamatergic inputs in dentate granule cells. J. Physiol. *592*, 67–86.

Hirzel, K., Müller, U., Latal, A.T., Hülsmann, S., Grudzinska, J., Seeliger, M.W., Betz, H., and Laube, B. (2006). Hyperekplexia phenotype of glycine receptor alpha1 subunit mutant mice identifies Zn(2+) as an essential endogenous modulator of glycinergic neurotransmission. Neuron *52*, 679–690.

Hosie, A.M., Dunne, E.L., Harvey, R.J., and Smart, T.G. (2003). Zinc-mediated inhibition of GABA(A) receptors: discrete binding sites underlie subtype specificity. Nat. Neurosci. *6*, 362–369.

Howell, G.A., Welch, M.G., and Frederickson, C.J. (1984). Stimulation-induced uptake and release of zinc in hippocampal slices. Nature *308*, 736–738.

Hunt, D.L., and Castillo, P.E. (2012). Synaptic plasticity of NMDA receptors: mechanisms and functional implications. Curr. Opin. Neurobiol. *22*, 496–508.

Jung, M.W., and McNaughton, B.L. (1993). Spatial selectivity of unit activity in the hippocampal granular layer. Hippocampus *3*, 165–182.

Karakas, E., Simorowski, N., and Furukawa, H. (2009). Structure of the zinc-bound amino-terminal domain of the NMDA receptor NR2B subunit. EMBO J. *28*, 3910–3920.

Kay, A.R. (2003). Evidence for chelatable zinc in the extracellular space of the hippocampus, but little evidence for synaptic release of Zn. J. Neurosci. *23*, 6847–6855.

Kay, A.R., and Tóth, K. (2008). Is zinc a neuromodulator? Sci. Signal. *1*, re3.

Kodirov, S.A., Takizawa, S., Joseph, J., Kandel, E.R., Shumyatsky, G.P., and Bolshakov, V.Y. (2006). Synaptically released zinc gates long-term potentiation in fear conditioning pathways. Proc. Natl. Acad. Sci. USA *103*, 15218–15223.

Koh, J.Y., Suh, S.W., Gwag, B.J., He, Y.Y., Hsu, C.Y., and Choi, D.W. (1996). The role of zinc in selective neuronal death after transient global cerebral ischemia. Science *272*, 1013–1016.

Komatsu, K., Kikuchi, K., Kojima, H., Urano, Y., and Nagano, T. (2005). Selective zinc sensor molecules with various affinities for Zn2+, revealing dynamics and regional distribution of synaptically released Zn2+ in hippocampal slices. J. Am. Chem. Soc. *127*, 10197–10204.

Kwon, H.B., and Castillo, P.E. (2008). Long-term potentiation selectively expressed by NMDA receptors at hippocampal mossy fiber synapses. Neuron *57*, 108–120.

Lavoie, N., Jeyaraju, D.V., Peralta, M.R., 3rd, Seress, L., Pellegrini, L., and Tóth, K. (2011). Vesicular zinc regulates the Ca2+ sensitivity of a subpopulation of presynaptic vesicles at hippocampal mossy fiber terminals. J. Neurosci. *31*, 18251–18265.

Lemke, J.R., Lal, D., Reinthaler, E.M., Steiner, I., Nothnagel, M., Alber, M., Geider, K., Laube, B., Schwake, M., Finsterwalder, K., et al. (2013). Mutations in GRIN2A cause idiopathic focal epilepsy with rolandic spikes. Nat. Genet. *45*, 1067–1072.

Li, Y., Hough, C.J., Suh, S.W., Sarvey, J.M., and Frederickson, C.J. (2001). Rapid translocation of Zn(2+) from presynaptic terminals into postsynaptic hippocampal neurons after physiological stimulation. J. Neurophysiol. *86*, 2597–2604.

Low, C.M., Zheng, F., Lyuboslavsky, P., and Traynelis, S.F. (2000). Molecular determinants of coordinated proton and zinc inhibition of N-methyl-D-aspartate NR1/NR2A receptors. Proc. Natl. Acad. Sci. USA *97*, 11062–11067.

Malenka, R.C., and Bear, M.F. (2004). LTP and LTD: an embarrassment of riches. Neuron *44*, 5–21.

Martel, G., Hevi, C., Friebely, O., Baybutt, T., and Shumyatsky, G.P. (2010). Zinc transporter 3 is involved in learned fear and extinction, but not in innate fear. Learn. Mem. *17*, 582–590.

Martel, G., Hevi, C., Kane-Goldsmith, N., and Shumyatsky, G.P. (2011). Zinc transporter ZnT3 is involved in memory dependent on the hippocampus and perirhinal cortex. Behav. Brain Res. *223*, 233–238.

Mody, I., Lambert, J.D., and Heinemann, U. (1987). Low extracellular magnesium induces epileptiform activity and spreading depression in rat hippocampal slices. J. Neurophysiol. *57*, 869–888.

Molnár, P., and Nadler, J.V. (2001). Synaptically-released zinc inhibits N-methyl-D-aspartate receptor activation at recurrent mossy fiber synapses. Brain Res. *910*, 205–207.

Mott, D.D., Benveniste, M., and Dingledine, R.J. (2008). pH-dependent inhibition of kainate receptors by zinc. J. Neurosci. *28*, 1659–1671.

Nozaki, C., Vergnano, A.M., Filliol, D., Ouagazzal, A.M., Le Goff, A., Carvalho, S., Reiss, D., Gaveriaux-Ruff, C., Neyton, J., Paoletti, P., and Kieffer, B.L. (2011). Zinc alleviates pain through high-affinity binding to the NMDA receptor NR2A subunit. Nat. Neurosci. *14*, 1017–1022.

Nydegger, I., Rumschik, S.M., and Kay, A.R. (2010). Zinc is externalized rather than released during synaptic transmission. ACS Chem Neurosci *1*, 728–736.

Oertner, T.G., Sabatini, B.L., Nimchinsky, E.A., and Svoboda, K. (2002). Facilitation at single synapses probed with optical quantal analysis. Nat. Neurosci. *5*, 657–664.

Pan, E., Zhang, X.A., Huang, Z., Krezel, A., Zhao, M., Tinberg, C.E., Lippard, S.J., and McNamara, J.O. (2011). Vesicular zinc promotes presynaptic and inhibits postsynaptic long-term potentiation of mossy fiber-CA3 synapse. Neuron *71*, 1116–1126.

Paoletti, P., Ascher, P., and Neyton, J. (1997). High-affinity zinc inhibition of NMDA NR1-NR2A receptors. J. Neurosci. *17*, 5711–5725.

Paoletti, P., Perin-Dureau, F., Fayyazuddin, A., Le Goff, A., Callebaut, I., and Neyton, J. (2000). Molecular organization of a zinc binding n-terminal modulatory domain in a NMDA receptor subunit. Neuron *28*, 911–925.

Paoletti, P., Vergnano, A.M., Barbour, B., and Casado, M. (2009). Zinc at glutamatergic synapses. Neuroscience *158*, 126–136.

Paoletti, P., Bellone, C., and Zhou, Q. (2013). NMDA receptor subunit diversity: impact on receptor properties, synaptic plasticity and disease. Nat. Rev. Neurosci. *14*, 383–400.

Perez-Rosello, T., Anderson, C.T., Schopfer, F.J., Zhao, Y., Gilad, D., Salvatore, S.R., Freeman, B.A., Hershfinkel, M., Aizenman, E., and Tzounopoulos, T. (2013). Synaptic Zn2+ inhibits neurotransmitter release by promoting endocannabinoid synthesis. J. Neurosci. *33*, 9259–9272.

Qian, J., and Noebels, J.L. (2005). Visualization of transmitter release with zinc fluorescence detection at the mouse hippocampal mossy fibre synapse. J. Physiol. *566*, 747–758.

Qian, J., and Noebels, J.L. (2006). Exocytosis of vesicular zinc reveals persistent depression of neurotransmitter release during metabotropic glutamate receptor long-term depression at the hippocampal CA3-CA1 synapse. J. Neurosci. *26*, 6089–6095.

Qian, J., Xu, K., Yoo, J., Chen, T.T., Andrews, G., and Noebels, J.L. (2011). Knockout of Zn transporters Zip-1 and Zip-3 attenuates seizure-induced CA1 neurodegeneration. J. Neurosci. *31*, 97–104.

Rachline, J., Perin-Dureau, F., Le Goff, A., Neyton, J., and Paoletti, P. (2005). The micromolar zinc-binding domain on the NMDA receptor subunit NR2B. J. Neurosci. *25*, 308–317.

Rebola, N., Lujan, R., Cunha, R.A., and Mulle, C. (2008). Adenosine A2A receptors are essential for long-term potentiation of NMDA-EPSCs at hippocampal mossy fiber synapses. Neuron *57*, 121–134.

Rollenhagen, A., Sätzler, K., Rodríguez, E.P., Jonas, P., Frotscher, M., and Lübke, J.H. (2007). Structural determinants of transmission at large hippocampal mossy fiber synapses. J. Neurosci. *27*, 10434–10444.

Sakimura, K., Kutsuwada, T., Ito, I., Manabe, T., Takayama, C., Kushiya, E., Yagi, T., Aizawa, S., Inoue, Y., Sugiyama, H., et al. (1995). Reduced hippocampal LTP and spatial learning in mice lacking NMDA receptor epsilon 1 subunit. Nature *373*, 151–155.

Savtchenko, L.P., Sylantyev, S., and Rusakov, D.A. (2013). Central synapses release a resource-efficient amount of glutamate. Nat. Neurosci. *16*, 10–12.

Schmitz, D., Mellor, J., and Nicoll, R.A. (2001). Presynaptic kainate receptor mediation of frequency facilitation at hippocampal mossy fiber synapses. Science *291*, 1972–1976.

Sensi, S.L., Paoletti, P., Bush, A.I., and Sekler, I. (2009). Zinc in the physiology and pathology of the CNS. Nat. Rev. Neurosci. *10*, 780–791.

Sensi, S.L., Paoletti, P., Koh, J.Y., Aizenman, E., Bush, A.I., and Hershfinkel, M. (2011). The neurophysiology and pathology of brain zinc. J. Neurosci. *31*, 16076–16085.

Sindreu, C., and Storm, D.R. (2011). Modulation of neuronal signal transduction and memory formation by synaptic zinc. Front Behav Neurosci *5*, 68.

Sindreu, C.B., Varoqui, H., Erickson, J.D., and Pérez-Clausell, J. (2003). Boutons containing vesicular zinc define a subpopulation of synapses with low AMPAR content in rat hippocampus. Cereb. Cortex *13*, 823–829.

Sindreu, C., Palmiter, R.D., and Storm, D.R. (2011). Zinc transporter ZnT-3 regulates presynaptic Erk1/2 signaling and hippocampus-dependent memory. Proc. Natl. Acad. Sci. USA *108*, 3366–3370.

Smart, T.G., Hosie, A.M., and Miller, P.S. (2004). Zn2+ ions: modulators of excitatory and inhibitory synaptic activity. Neuroscientist *10*, 432–442.

Sylantyev, S., Savtchenko, L.P., Niu, Y.P., Ivanov, A.I., Jensen, T.P., Kullmann, D.M., Xiao, M.Y., and Rusakov, D.A. (2008). Electric fields due to synaptic currents sharpen excitatory transmission. Science *319*, 1845–1849.

Sylantyev, S., Jensen, T.P., Ross, R.A., and Rusakov, D.A. (2013). Cannabinoid- and lysophosphatidylinositol-sensitive receptor GPR55 boosts neurotransmitter release at central synapses. Proc. Natl. Acad. Sci. USA *110*, 5193–5198.

Tovar, K.R., and Westbrook, G.L. (2012). Amino-terminal ligands prolong NMDA Receptor-mediated EPSCs. J. Neurosci. *32*, 8065–8073.

Traynelis, S.F., Burgess, M.F., Zheng, F., Lyuboslavsky, P., and Powers, J.L. (1998). Control of voltage-independent zinc inhibition of NMDA receptors by the NR1 subunit. J. Neurosci. *18*, 6163–6175.

Ueno, S., Tsukamoto, M., Hirano, T., Kikuchi, K., Yamada, M.K., Nishiyama, N., Nagano, T., Matsuki, N., and Ikegaya, Y. (2002). Mossy fiber Zn^{2+} spillover modulates heterosynaptic N-methyl-D-aspartate receptor activity in hippocampal CA3 circuits. J. Cell Biol. *158*, 215–220.

Veran, J., Kumar, J., Pinheiro, P.S., Athané, A., Mayer, M.L., Perrais, D., and Mulle, C. (2012). Zinc potentiates GluK3 glutamate receptor function by stabilizing the ligand binding domain dimer interface. Neuron *76*, 565–578.

Vogt, K., Mellor, J., Tong, G., and Nicoll, R. (2000). The actions of synaptically released zinc at hippocampal mossy fiber synapses. Neuron *26*, 187–196.

Watanabe, M., Fukaya, M., Sakimura, K., Manabe, T., Mishina, M., and Inoue, Y. (1998). Selective scarcity of NMDA receptor channel subunits in the stratum lucidum (mossy fibre-recipient layer) of the mouse hippocampal CA3 subfield. Eur. J. Neurosci. *10*, 478–487.

Wemmie, J.A., Chen, J., Askwith, C.C., Hruska-Hageman, A.M., Price, M.P., Nolan, B.C., Yoder, P.G., Lamani, E., Hoshi, T., Freeman, J.H., Jr., and Welsh, M.J. (2002). The acid-activated ion channel ASIC contributes to synaptic plasticity, learning, and memory. Neuron *34*, 463–477.

Wenzel, H.J., Cole, T.B., Born, D.E., Schwartzkroin, P.A., and Palmiter, R.D. (1997). Ultrastructural localization of zinc transporter-3 (ZnT-3) to synaptic vesicle membranes within mossy fiber boutons in the hippocampus of mouse and monkey. Proc. Natl. Acad. Sci. USA *94*, 12676–12681.

Williams, K. (1996). Separating dual effects of zinc at recombinant N-methyl-D-aspartate receptors. Neurosci. Lett. *215*, 9–12.

Zheng, F., Erreger, K., Low, C.M., Banke, T., Lee, C.J., Conn, P.J., and Traynelis, S.F. (2001). Allosteric interaction between the amino terminal domain and the ligand binding domain of NR2A. Nat. Neurosci. *4*, 894–901.